

Article

Decontamination of Food Packages from SARS-CoV-2 RNA with a Cold Plasma-Assisted System

Filippo Capelli^{1,2}, Silvia Tappi^{3,4,*}, Tommaso Gritti⁵, Ana Cristina de Aguiar Saldanha Pinheiro³, Romolo Laurita^{1,2,*}, Urszula Tylewicz^{3,4}, Francesco Spataro³, Giacomo Braschi³, Rosalba Lanciotti^{3,4}, Federico Gómez Galindo⁶, Valentina Siracusa⁷, Santina Romani^{3,4}, Matteo Gherardi^{1,2}, Vittorio Colombo^{1,2,4}, Vittorio Sambri^{5,8} and Pietro Rocculi^{3,4}

- ¹ Department of Industrial Engineering (DIN), University of Bologna, 40136 Bologna, Italy; filippo.capelli@unibo.it (F.C.); matteo.gherardi@unibo.it (M.G.); vittorio.colombo@unibo.it (V.C.)
- ² Interdepartmental Center for Industrial Research for Advanced Mechanics and Materials, University of Bologna, 40136 Bologna, Italy
- ³ Department of Agricultural and Food Sciences, University of Bologna, 47521 Cesena, Italy; anacristin.deaguiar2@unibo.it (A.C.d.A.S.P.); urszula.tylewicz@unibo.it (U.T.); francesco.spataro4@unibo.it (F.S.); giacomo.braschi2@unibo.it (G.B.); rosalba.lanciotti@unibo.it (R.L.); santina.romani2@unibo.it (S.R.); pietero.roculli3@unibo.it (P.R.)
- ⁴ Interdepartmental Centre for Agri-Food Industrial Research, University of Bologna, 47521 Cesena, Italy
- ⁵ Department of Experimental, Diagnostic and Specialty Medicine, University of Bologna, 40136 Bologna, Italy; tommaso.gritti2@unibo.it (T.G.); vittorio.sambri@unibo.it (V.S.)
- ⁶ Department of Food Technology, Engineering and Nutrition, Lund University, Naturvetarvägen 14, SE- 22362 Lund, Sweden; federico.gomez@food.lth.se
- ⁷ Department of Chemical Science, Viale A. Doria 6, 95125 Catania, Italy; vsiracus@dmfci.unict.it
- ⁸ Unit of Microbiology, The Great Romagna Hub Laboratory, 47522 Pievesestina, Italy
- * Correspondence: silvia.tappi2@unibo.it (S.T.); romolo.laurita@unibo.it (R.L.)



Citation: Capelli, F.; Tappi, S.; Gritti, T.; de Aguiar Saldanha Pinheiro, A.C.; Laurita, R.; Tylewicz, U.; Spataro, F.; Braschi, G.; Lanciotti, R.; Gómez Galindo, F.; et al. Decontamination of Food Packages from SARS-CoV-2 RNA with a Cold Plasma-Assisted System. *Appl. Sci.* **2021**, *11*, 4177. <https://doi.org/10.3390/app11094177>

Academic Editor: Gyungsoon Park

Received: 13 April 2021

Accepted: 30 April 2021

Published: 4 May 2021

Publisher's Note: MDPI stays neutral with regard to jurisdictional claims in published maps and institutional affiliations.



Copyright: © 2021 by the authors. Licensee MDPI, Basel, Switzerland. This article is an open access article distributed under the terms and conditions of the Creative Commons Attribution (CC BY) license (<https://creativecommons.org/licenses/by/4.0/>).

Featured Application: The actual emergency linked to the pandemic from SARS-CoV-2 brought about the need of a new critical control point (CCP) linked to the external packaging contamination of packaged foods. Therefore, cold plasma technology is of great interest in handling this new criticality as it can be applied in both the production and distribution steps of the food supply chain.

Abstract: The accidental contamination of food and food packaging surfaces with SARS-CoV-2 is of increasing concern among scientists and consumers, particularly in relation to fresh foods that are consumed without further cooking. The use of chemical sanitizers is often not suitable for these kinds of commodities; therefore, a non-thermal sanitation technology could help to increase safety in relation to the food supply chain. Cold plasma has proven to be a promising strategy for virus inactivation. This research is aimed at evaluating the ability of a cold plasma sanitation system to inactivate SARS-CoV-2 RNA on packaged foods. Two different plastic materials were investigated and subjected to 5- and 10-min exposure to plasma after experimental inoculum of the RNA. In addition to viral degradation, possible changes in the performance of the materials were evaluated. Shelf-life of the foods, after exposure of the packages to plasma, was also investigated. Results showed that 10 min of exposure was sufficient to almost completely eliminate the viral RNA from package surfaces. The treatment did not produce any significant variation in packaging material performance or the shelf-life of the tested packaged products, indicating the potentiality of this treatment for the decontamination of packaged products.

Keywords: Covid-19; packaging materials; viral RNA; cold plasma; food quality; food shelf-life; food safety

1. Introduction

The COVID-19 pandemic was caused by the SARS-CoV-2 virus, a member of the *Coronaviridae* family whose genome is a single-stranded RNA molecule [1]. The spread of SARS-CoV-2 in humans occurs mainly by air due to sneezing, coughing, and exhaling, or via contaminated surfaces and objects, although these seem to be less important in sustaining viral diffusion [2]. However, consumers have raised concerns about the possibility of transmission through food or its packaging.

Different risk assessments have been carried out by food safety agencies to determine whether food or food contact materials represent a significant risk to food safety in relation to SARS-CoV-2 infection. The European Food Safety Agency (EFSA) has excluded the possibility of transmission of the virus through the digestive tract; however, the possibility that the respiratory tract could become infected during the ingestion of contaminated food or water cannot be completely excluded. An infected person can contaminate food by handling it with dirty hands or through droplets from coughing or sneezing. Like other known coronaviruses, this virus is sensitive to heat treatment and cooking temperatures above 60 °C. Indeed, exposure of foods to 63 °C for 4 min (used for the preparation of hot food in collective catering) has been shown to be sufficient to inactivate the virus [3].

Hence, SARS-CoV-2 represents a risk factor, especially for fresh food consumed without prior cooking, for which good manufacturing practices are the only way to prevent contamination. Regarding the persistence of the virus on the surface of packaging materials, an analysis of 23 scientific studies revealed that some human coronaviruses can persist on metal, glass, or plastic for anywhere from a few hours up to nine days, depending on the material [4].

Therefore, the accidental contamination by SARS-CoV-2 of the external surfaces of the materials used for the packaging, processing, and handling of food (equipment and tools) represents a new and crucial issue to be carefully evaluated. Current WHO guidance states that “thoroughly cleaning environmental surfaces with water and detergent and applying commonly used hospital-grade disinfectants (such as sodium hypochlorite) are effective and sufficient” [5]. Disinfectants are very important in the control and inactivation of microorganisms on various inanimate surfaces [5–7]. However, they can leave harmful residues on surfaces in contact with food. In addition, many of them lose their antimicrobial activities in the presence of organic matter. Furthermore, their use is not allowed on specific types of packaging materials, and their effect is often nil when chemical sanitation procedures are performed by untrained people, such as consumers.

A non-thermal sanitization technique could guarantee a further reduction in the risk of SARS-CoV-2 transmission by minimally processed foods, in cases of accidental contamination during the handling of food during the preparation phase and/or of its packaging during distribution and sale. Among the emerging non-thermal sanitization technologies, cold atmospheric pressure plasma (CAP) is one of the most promising. Obtainable by applying a sufficiently high electric field in the air, CAP contains numerous reactive species in addition to O₃ (O, OH, NO, and NO₂) and also UV, all agents with known strong antimicrobial power. There are numerous studies on the use of CAP against viruses of non-food origin (flu and parainfluenza viruses, adenovirus, corneal herpes simplex virus, etc.) [8–10] and SARS-CoV-2 RNA [11]. Recently, the plasma effect was also successfully tested against SARS-CoV-2 on some inanimate surfaces such as plastic, metal, cardboard, and different types of leather for sports use [12]. CAP acts according to different mechanisms, causing damage to the capsid structure and viral RNA due to its high oxidizing power. However, while microbial inactivation on packaging materials has been extensively tested, the virucidal effect has only been assessed on surfaces of few food-contact materials, such as stainless steel. On the other hand, any treatment applied to food packaging materials might bring changes to their physical and chemical material properties, thus affecting their functionality. Therefore, it is fundamental to assess how exposure to plasma affects the main functional and technological performance of the materials, and to verify that it has no negative effect on the shelf-life of packaged foods.

This research is a first study to test the effectiveness of a newly developed cold plasma sanitation system as strategy to decontaminate food packages from SARS-CoV-2 RNA, which plays a major role in infection, as an introductory step towards a more complex study to assess the potential antiviral activity of CAP toward SARS-CoV-2. To this aim, after characterization of the plasma discharge generated by the developed prototype, viral RNA was experimentally inoculated on two food packaging materials and then subjected to CAP treatment. The effect on the RNA structure was evaluated together with the main properties of the materials and the shelf-life of the packaged products.

2. Materials and Methods

2.1. Plasma System

A schematic of the plasma system adopted in this study, Plasma Assisted Sanitation System (PASS), developed by AlmaPlasma srl, is shown in Figure 1. PASS is composed of an SDBD (surface dielectric barrier discharge) plasma source, a treatment chamber, a cooling system, and a high-voltage generator. The SDBD consists of a mica dielectric layer (2 mm thick) interposed between an air-cooled high-voltage (HV) aluminum electrode and a grounded electrode (AISI 316L rhomboid mesh). The treatment chamber is made of poly(methyl methacrylate) (PMMA) and has two optical accesses (quartz windows) to allow optical spectroscopy; when the SDBD is placed on the top of the treatment chamber a closed volume is defined. This treatment volume can be reduced by means of PMMA fillings, resulting in three different treatment volumes (Table 1).

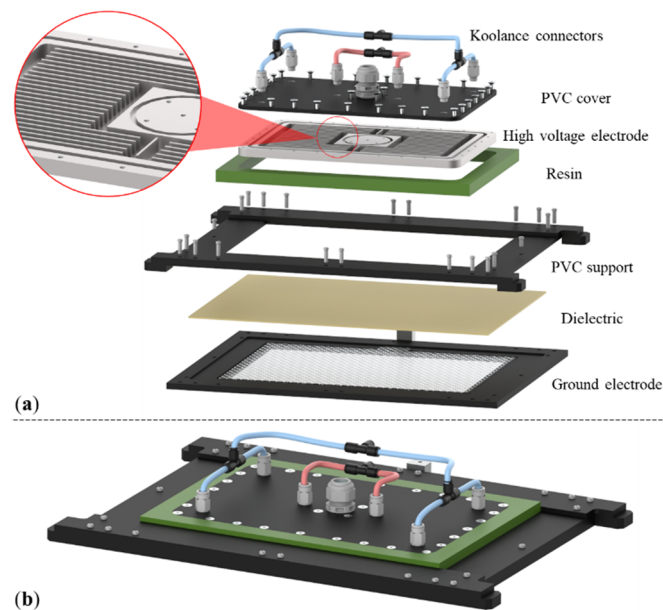


Figure 1. 3D schematic of the SDBD plasma source used in the experimental activities: (a) exploded and (b) assembled views of the plasma source

Table 1. Available treatment volumes defined using different PMMA fillings.

Volume	Volume $\times 10^3$ (cm ³)
V1	2.60
V2	5.21
V3	6.51

CAP was homogeneously generated on the surface of the mesh on an area of around 551 cm². The device, operating in environmental air (relative humidity in the range 20–40%), was driven by a micropulsed generator (AlmaPULSE, AlmaPlasma srl, Bologna, Italy), allowing the application of 1–20 kV, with a frequency in the 1–20 kHz range, and

a tunable duty cycle (1–100%). Two discharge times, considered the time for which the generator was kept on, were tested: 10 and 20 min. To evaluate the surface power density (SPD) delivered to the plasma source, voltage and current waveforms were recorded by means of a high-voltage probe (Tektronix P6015A) and a current probe (Pearson 6585) connected to an oscilloscope (Tektronix DPO40034). The power density was evaluated using the following formula:

$$SPD = \frac{1}{A} \cdot \frac{1}{T} \int V \cdot Idt \quad (1)$$

where V is the applied voltage, I is the current, T is the period, and A is the active surface of the mesh. The SPD was calculated by averaging three measurements, each taking into account 400 microseconds of plasma discharge (i.e., two full voltage periods) with an acquisition rate of 0.25 giga samples per second.

The plasma source was operated imposing a voltage of 6.00 kV at a frequency of 5.00 kHz with a fixed duty cycle (DC = 100%).

The mesh temperature was measured during the discharge time by means of a fiber optical temperature sensor (opSense, OTG series), placed inside the investigated volume, and data were recorded every 0.05 s.

2.2. Packaging Materials and Food Products

Polyethylene terephthalate (PET) trays (350 microns thick) and polypropylene (PP) film (69 microns thick) were selected as representative of the main materials used for fresh food packaging. The former was rigid, while the latter was a flexible material. Both materials were provided by local food industry (Emilia-Romagna, Italy).

For the evaluation of virus inactivation, square pieces of PP and PET (~1 cm²) were used for the inoculum of viral RNA and subjected to CAP treatment.

For the shelf-life study of food products, two different batches of fresh-cut unpeeled apples (cultivar Fuji) were packed with PP pouches (net weight ≈ 80g) and PET trays (net weight ≈ 150 g). Packaged food products were provided by local food industry (Emilia-Romagna, Italy)

2.3. Contamination of Materials with SARS-CoV-2 RNA and Analysis

The SARS-CoV-2 RNA extract used was purchased from Vircell (Granada, Spain). This RNA preparation was obtained from SARS-CoV-2 (lineage B1) grown in vitro in VERO E6 cells, extracted and stored at −80 °C until use.

Packaging material squares (area ~1 cm²) were used as a model of contact surfaces. These pieces were sterilized by immersion in H₂O₂ at room temperature for 30 s.

Packaging materials were contaminated using the Sars-CoV-2 RNA extract previously described. Contamination of both packaging materials was performed by spreading two 5 µL drops of RNA extract on each piece, followed by exposure to air, as a positive untreated control (K), or immediate CAP treatment.

2.4. Plasma Treatment

Both packaging materials and packaged products were exposed to CAP treatment for two treatment times (5 and 10 min).

Square material samples with and without RNA inoculum were placed on Petri dishes and placed in the PASS treatment chamber at treatment volume V3.

Treatment of the packaged products without inoculum was carried out separately. Two packages containing fresh-cut apples, as described in Section 2.3, were subjected to CAP for 5 (P5) and 10 (P10) min and compared with the untreated sample (C). For each type of sample, 12 replicates were obtained and used for shelf-life tests.

2.5. Analytical Determinations

2.5.1. Setup for Optical Absorption Spectroscopy (OAS) and Data Processing

The setup for OAS is the same as that used by Simoncelli et al. [13] and is schematically represented in Figure 2. A deuterium-halogen lamp, characterized by a broad band spectrum from UV to NIR radiation, was used as a light source. With the aim of investigating the plasma afterglow, the light beam was focused by means of optical fibers and fused silica lenses (50 mm of focus length) to achieve a parallel beam which passed under the mesh and was collected by a 500 mm spectrometer (Acton SP2500i, Princeton Instruments) to spectrally resolve the light beam in the UV, VIS, and near infrared (NIR) regions. The width of the inlet slit of the spectrometer was fixed at 50 μm for OAS acquisitions, and a grating with a resolution of 150 mm^{-1} was used. A photomultiplier tube (PMT, Princeton Instruments PD439) connected to a fast oscilloscope (Tektronix DPO40034) was used as detector, allowing fast acquisitions with a time resolution of 40 ms. The PMT amplification factor was kept constant for all acquisitions. In order to ensure identical initial conditions, the discharge chamber was opened and flushed for 30 s with fresh air prior to every measurement.

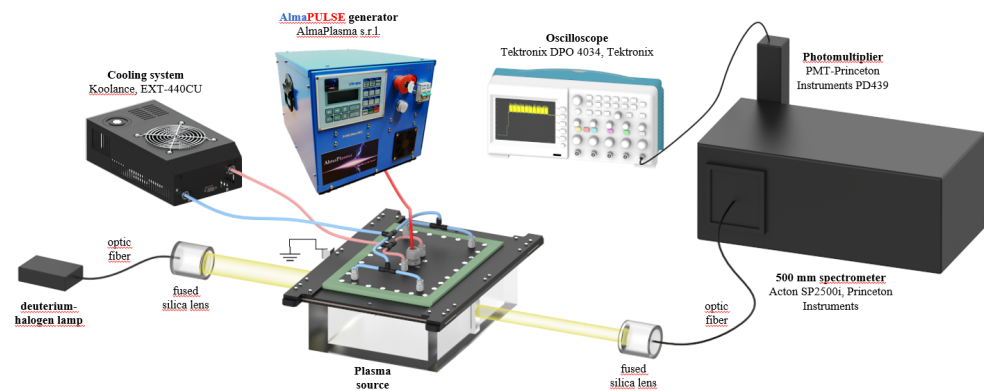


Figure 2. Schematic of the experimental setup for optical absorption spectroscopy.

In order to quantitatively evaluate the species' concentrations from absorption measurements, the Lambert–Beer law was taken into account:

$$\frac{I}{I_0} = e^{(-L\sigma n)} \quad (2)$$

where I/I_0 is the ratio between the initial light intensity I_0 and the light intensity I after an optical path length L , and n is the concentration of absorbers. The absorption cross-section σ is a function of the wavelength ($\sigma = \sigma(\lambda)$).

In general, when N species absorb at the same λ_j wavelength, the Lambert–Beer equation can be re-written as:

$$\frac{I}{I_0} \Big|_j = e^{(-L \sum_{i=1}^N \sigma_{i,j} n_i)} \quad (3)$$

where $\sigma_{i,j}$ represents the absorption cross-section of the i -species at λ_j and the ratio between the light intensities I and I_0 is referred to the j -wavelength. The concentration n of each absorbing species can thus be obtained from the following expression, where the suffix k indicates a generic absorber:

$$n_k = -\frac{1}{L\sigma_{k,j}} \ln \left(\frac{I}{I_0} \Big|_j \right) - \sum_{i \neq k} \frac{\sigma_{i,j}}{\sigma_{k,j}} n_i \quad (4)$$

The wavelengths selected to perform the study and the corresponding absorption cross-sections for O_3 and NO_2 as absorbers are reported in Table 2. These wavelengths were

defined, in accordance with Moiseev [14], to maximize the absorption of the molecules relevant to our study while minimizing the contribution, and thus the disturbance, of other absorbing molecules.

Table 2. Absorption cross-sections in cm^2 of the species of interest at each selected wavelength.

Selected Wavelength	O ₃ Cross-Section	NO ₂ Cross-Section
253 ± 1.2 nm	$(1.12 \pm 0.02) \times 10^{-17}$	$(1.1 \pm 0.3) \times 10^{-20}$
400 ± 1.2 nm	$(1.12 \pm 0.08) \times 10^{-23}$	$(6.4 \pm 0.2) \times 10^{-19}$

For all experiments, the optical path length L was 21 cm and the contributions of background radiation and spontaneous plasma emission were duly taken into account in the data processing, subtracting them from the acquired values of I and I_0 .

2.5.2. SARS-CoV-2 RNA Analysis

After treatment, the inoculated drops were retrieved, collected, and stored at 4 °C in sterile RNase-free vials for less than 24 h.

The RT-PCR reaction was performed using n-COVID Allplex SARS-CoV-2 assay mix (SeeGene, Seoul, Korea), dispensed by the Starlet platform (Hamilton, USA). RT-PCR was performed using a CFX96 thermal cycler (Bio-Rad, Hercules, CA, USA). RT-PCR results were analyzed using the SeeGene Viewer Plus V1 (SeeGene) software.

The applied PCR method is able to detect three sequence targets (E, RdRp, and N) in the SARS-CoV-2 genome.

PCR data were shown as a percentage reduction in detected RNA between treated and positive control (K) samples, using Ct values for each target:

$$\%RNA\ reduction = \frac{"Treated\ Sample\ Ct\ Value" - "K\ Ct\ Value"}{40 - "K\ Ct\ Value"} \quad (5)$$

In this context, we approximated 100% of eliminated RNA to the experimental condition's upper detection limit (40 Ct) and approximated 0% of eliminated RNA to the Ct values observed for each target in the K samples (K Ct Value).

2.5.3. Packaging Material Performance

Packaging materials were tested for gas permeability, thermal properties, and global migration before and immediately after the application of plasma treatment.

Permeability measurement was performed using a manometric method, by the evaluation of gas transmission rate (GTR, expressed in cm^3/m^2 day bar) for O₂ and CO₂ on a permeance testing device, type GDP-C (Brugger Feinmechanik GmbH, Munchen, Germany), in accordance with ASTM 1434 (standard test method for determining gas permeability characteristics of plastic film and sheeting, 2009), DIN 53536 (gas permeability determination), ISO 15105-1 (plastic film and sheeting determination of gas transmission rate—Part I: Differential pressure methods, 2007), and the Gas Permeability Testing Manual, 2008 (Registergericht München HRB 77020, Brugger Feinmechanik GmbH). A mean value from triplicate experiments was considered [15–17].

Film and tray thickness (δ) was measured using a Sample Thickness Tester DM-G with a digital dial indicator (MarCator 1086 model, Mahr GmbH, Esslingen, Germany) and associated DM-G software. The reading was made twice per second, with a resolution of 0.001 mm. The minimum, maximum, and average of each reading was recorded in triplicate, in 10 different positions for each film at room temperature, and reported as mean thickness value, expressed in microns.

Thermal properties were evaluated by differential scanning calorimetry (DSC) using a DSC model Q20 (TA Instrument, New Castle, DE, USA) equipped with a cooling unit (TA Refrigerated Cooling System 90). The calibration of the instrument was performed

with distilled water (T_m 0.0 °C), indium (T_m 156.60 °C), and zinc (T_m 419.47 °C) under a dry nitrogen flow of 50 mL min⁻¹. Samples of about 10 mg were weighed in hermetically closed 50 µL aluminum DSC capsules. The samples were first equilibrated at a temperature of -30 °C for 5 min, then heated, with a first scanning rate of 10 °C/min, from -30 to 180 °C (for PP) and 280 °C (for PET) and then, after an isotherm of 3 min at 180 °C or 280 °C, samples were cooled to -30 °C at a rate of 80 °C/min. After a second isothermal step of 3 min at -30 °C, a second heating was performed with the same parameters as the first one (second scan). Peaks were integrated with TA Universal Analysis software (TA Instrument, New Castle, DE, USA) to determine the melting temperature (T_m) as the peak value of the endothermic phenomena in the DSC curve, and the melting enthalpy (ΔH_m) from the area of the DSC endothermic peak. T_m and ΔH_m values were collected from the first scan.

The crystallinity percentage (X_c) was calculated through the following equation:

$$X_c (\%) = (\Delta H_m / \Delta H_m^*) 100$$

where ΔH_m is the experimental melting enthalpy and ΔH_m^* is the melting enthalpy of the 100% crystalline polymer, equal to 207.1 J/g for PP and 140.1 J/g for PET [18].

Overall migration test was performed according to UE 10/2011. For each polymer type, samples of 3 dm² were prepared and placed in a hermetically closed glass jar containing 100 mL of food simulant for 10 days at 40 °C. Acetic acid at 3% (*w/v*) and distilled water were used as food simulants. After 10 days of contact between the polymer and the simulants, the latter were evaporated and the glass jar was weighted. The overall migration was calculated according to the following equation:

$$OM = (m_f - m_i) / S$$

where OM is the overall migration (mg/dm²), m_i and m_f are, respectively, the initial and final weight of the glass jar (mg), and S is the surface area of the polymer samples (dm²).

2.5.4. Product Shelf-Life

After the treatment, the packaged fresh-cut apple samples were stored at 8 ± 1 °C and analytical determinations were carried out after 0, 3, 6, and 9 days of storage, considering at least three packages each time.

The concentration of O₂ and CO₂ (%) in the package headspace was determined by a gas analyzer (MFA III S/L gas analyzer, Witt-Gasetechnik, Witten, Germany). The measurements were performed on at least three packages for each sample.

Microbiological analyses were performed after 1, 3, 6, and 9 days of refrigerated storage, in order to take into account the specific growth kinetics of the investigated microorganisms. Each sample was analyzed in triplicate. Microbial groups considered as spoilage indicators were total mesophilic counts (TMC), *Lactobacillus* spp., total yeasts, and molds. Fifty grams of cut apples were suspended 1:1 (*p/v*), serially diluted using physiological saline solution (0.9% NaCl), and 1 mL or 100 µL were included or spread in different selective or complex culture media, such as plate count agar (PCA) (Oxoid-Thermofisher, Milano, Italy) for TMC; de Man, Rogosa, and Sharpe agar (MRS) (Oxoid-Thermofisher, Milano, Italy) supplemented with cyclo-heximide (0.2% *p/v*) (Sigma-Aldrich, Milano, Italy) for *Lactobacillus* spp.; and yeast extract, peptone, dextrose agar (YPD) for total yeast and mold counts. Plates were incubated for 24 or 48 h at 30 °C for the counts of total mesophilic bacteria, yeasts, and molds, and at 37 °C for *Lactobacilli* load determination.

Titrate acidity (TA) was determined by titration with NaOH 0.1 N until pH 8.1 was reached [19], and expressed in g of malic acid per 100 g of fresh weight. For each sample, TA was determined in triplicate on the juice obtained by \approx 300 g of apple slices with a food processor.

Surface color of fresh-cut apple samples was measured with a Chroma Meter CR-400 reflectance colorimeter (Minolta Italia, Milano, Italy) using the D65 illuminant and a 10°

standard observer. The lightness (L^*) and red index (a^*) of the CIELAB scale were measured according to the lab scale established by Commission Internationale de l'Éclairage (CIE, 2001). Results were expressed as an average of 15 readings for each set of samples.

Texture of samples was assessed through a penetration test performed using a Texture Analyser TA-HDi500 (Stable Micro Systems, Surrey, UK) equipped with a 50-N load cell and a 6-mm diameter stainless steel cylindrical probe. The test speed was set at 0.5 mm s^{-1} and the maximum deformation at 90%. Fifteen measurements were carried out from each set of samples and the first peak force (N) was extracted from the acquired curves.

2.6. Statistical Analysis

Data were processed using STATISTICA 8 software (Version 8.0; Statsoft, Tulsa, OK, USA). Differences in relation to the plasma treatment applied were considered significant ($p < 0.05$) on the basis of ANOVA and Tukey's HSD post-hoc test.

3. Results

3.1. Electrical Characterization and Gas Temperature Measurement

An example of recorded voltage and current waveforms, used for power calculation, is shown in Figure 3A.

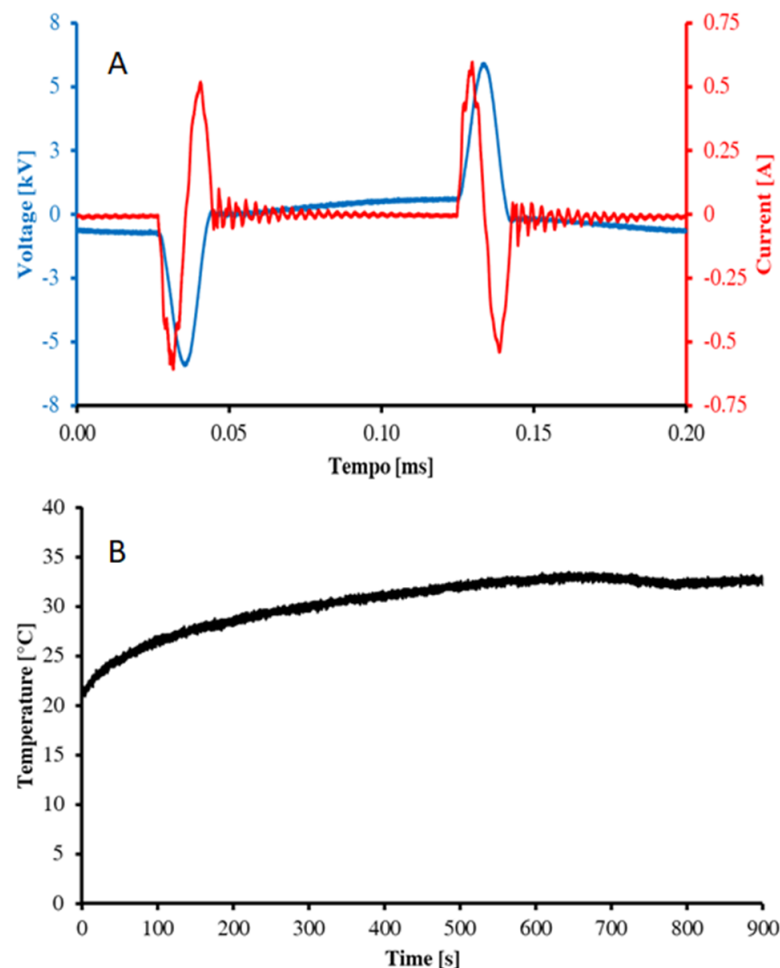


Figure 3. Voltage (blue) and current (red) waveforms (A) and gas temperature measurements during 900 s of discharge (B).

The SPD absorbed by the SDBD was $6.81 \pm 0.02 \times 10^{-2} \text{ W/cm}^2$. The SPD is a key parameter of CAP treatment in air because it is known to directly affect the production of RONS [20,21].

This value of SPD was measured using each available treatment volume; as expected, no difference could be detected.

Figure 3B highlights the limited increase in temperature in the afterglow region during the discharge time. The maximum measured gas temperature was below 34 °C.

3.2. O₃ and NO₂ Kinetics

The kinetics of ozone generation obtained by varying the treatment volume are shown in Figure 4. At first, the ozone kinetics showed a continuous increase in O₃ concentration over time; after reaching a maximum value, the concentrations remained constant until the end of the treatment. It must be highlighted that, while the O₃ maximum values were almost the same for the different treatment volumes (~1700 ppm), the time needed to reach that maximum value was different for the three investigated cases. It can be noted that the larger the volume, the slower the maximum concentration was reached; moreover, larger volumes produced slightly lower concentration peaks. Finally, it must be underlined that using the larger volume created an anomalous trend during the initial 50 s of treatment; however, this phenomenon was observed in each repetition.

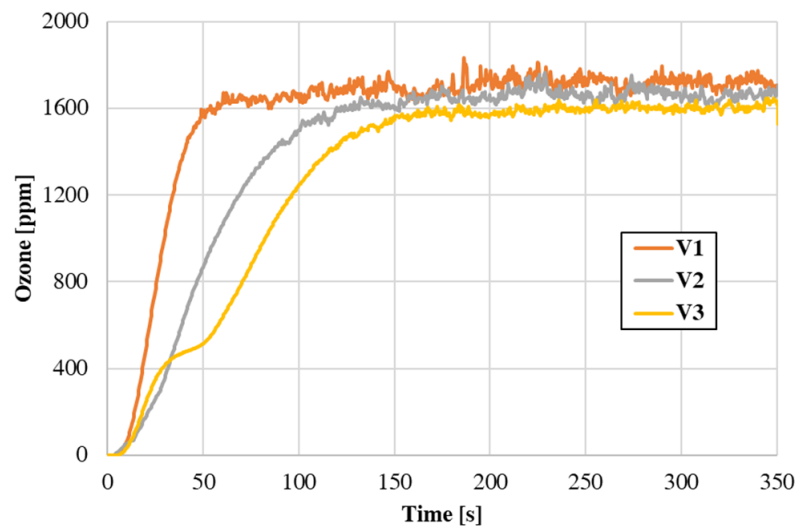


Figure 4. O₃ concentration kinetics for different treatment volumes (V1, V2, V3).

The time needed in the different cases to overcome the threshold of 1600 ppm ozone concentration, and the maximum concentration reached during treatments, are reported in Table 3.

Table 3. Time needed to overcome the threshold of 1600 ppm of ozone concentration for different treatment volumes and maximum O₃ concentration reached during treatment.

Volume #	Treatment Time to Overcome 1600 ppm of O ₃ [s]	Maximum O ₃ Concentration [ppm]
V1	56.8	1833.4
V2	122.0	1767.0
V3	167.2	1648.5

NO₂ concentration was not detectable, which is in good agreement with the literature [13,14,20,21]. It is known that for small values of SPD, reactions leading to the production of nitrogen oxides are disadvantaged and therefore negligible (ozone regime). For increasing values of SPD, the production of nitrogen oxides is favored, resulting in the destruction of ozone (nitrogen oxides regime). Among the above-mentioned papers, different values of SPD can be found to define the threshold which divides ozone regime and nitrogen oxides regime. Even if the SPD threshold changes with the plasma source, all

the values reported in the literature are close to 0.1 W/cm^2 , which is consistently larger than our SPD. Both SPD and OAS measurements suggest that the process studied in this work occurs in ozone regime, regardless of the treatment volume used, which in fact does not affect the SPD.

3.3. SARS-CoV-2 RNA Degradation

The results of the degradation of viral RNA on PP and PET after 5 and 10 min of exposure to air (K5 and K10) and CAP (P5 and P10) for the three analyzed RNA targets (E, RdRP, and N) are shown in Figure 5. The viral RNA reduction promoted only by air exposure for both the packaging materials investigated was very limited, as reported for K5 and K10 samples. After 5 min of CAP treatment, for both packaging materials, a significant but small reduction in detected RNA was observed, of about 10 and 16% for PP and PET, respectively. On the contrary, CAP treatment for 10 min completely degraded the RNA molecules, whose concentration resulted below the detection limits for each target sequence detected by this PCR method.

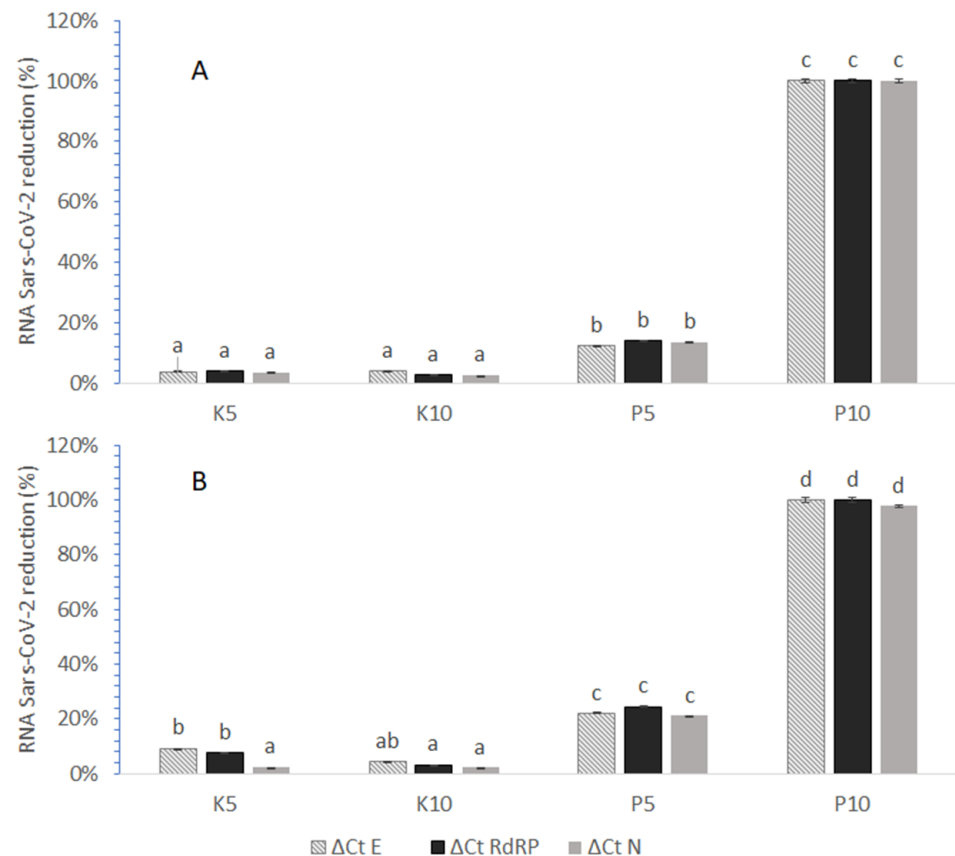


Figure 5. Percent reduction in SARS-CoV-2 RNA in terms of the three sequence targets investigated (E, RdRP, and N, represented respectively as light gray, black, and dark gray bars) in PP (A) and PET (B) samples treated for 5 (P5) and 10 min (P10), compared with their positive controls (K5 and K10). Different letters indicate significant differences among values related to the same packaging materials.

The damage of viral nucleic acid, as evidenced in different studies, seems to be due principally to the action of reactive oxygen and nitrogen (RONS) species. In this direction, the active species produced during the CAP treatment, being able to damage the genetic material of the virus, can make viral cells unable to promote the infection, considering that the genetic material is necessary for the virus genome translation and replication. The slight difference observed between CAP performance on PP and PET, treated for 5 min, may suggest that the interaction between reactive species and viral genetic material is affected by the matrix.

There is also evidence that the high oxidative power of CAP treatment can disrupt viral integrity at both structural and genomic levels, and even damage the capsid structure, which could drive the loss of viral functionality [22]. For this reason, further studies will be undertaken in due course in our lab in order to assess the CAP effect on the SARS-CoV-2 virus whole capsid, using combinations of methods able to assess both of these different types of actions.

3.4. Packaging Performance

GTR values related to O₂ and CO₂ permeability were, respectively, 913 ± 0.6 and 2230 ± 17 cm³/m² day bar for untreated PP. The CAP treatment, either for 5 or 10 min, did not induce any significant changes on these parameters (data not reported), indicating that the controlled exposure of polymeric films to gas plasma did not produce important effects on their performance in terms of gas barrier properties.

Table 4 shows the measured thermal properties of PP and PET before and after plasma exposure. The melting enthalpy of PP film did not change after exposure to gas plasma. Crystallinity percentage values ranging between 16.2–17.8% from the first scan, and 15.8–16.7% from the second scan, were recorded. A slight but not statistically significant temperature increase was measured during the second scans, highlighting the great thermal stability of PP films.

Table 4. Thermal properties of untreated (C) and cold plasma-treated PP and PET samples for 5 (P5) and 10 (P10) min.

	First Heating			Second Heating		
	ΔH_m (J/g)	T_m (°C)	X_c (%)	ΔH_m (J/g)	T_m (°C)	X_c (%)
PP						
C	33.6 ^a ± 5.8	164.8 ^a ± 0.6	16.2 ^a ± 2.8	33.0 ^a ± 4.8	165.5 ^a ± 0.4	15.9 ^a ± 2.3
P5	36.9 ^a ± 1.5	164.2 ^a ± 0.6	17.8 ^a ± 0.7	34.6 ^a ± 1.6	165.4 ^a ± 0.1	16.7 ^a ± 0.8
P10	34.8 ^a ± 3.8	164.8 ^a ± 0.7	16.8 ^a ± 1.8	32.7 ^a ± 3.3	165.5 ^a ± 0.1	15.8 ^a ± 1.6
PET						
C	44.7 ^a ± 7.8	248.8 ^a ± 0.5	27.6 ^a ± 4.8	31.9 ^a ± 5.6	248.6 ^a ± 0.3	31.9 ^a ± 5.5
P5	51.2 ^a ± 9.1	249.6 ^a ± 0.2	31.3 ^a ± 9.2	36.5 ^a ± 7.2	248.3 ^a ± 0.2	36.5 ^a ± 7.2
P10	52.3 ^a ± 9.3	249.6 ^a ± 0.1	32.9 ^a ± 9.8	37.3 ^a ± 6.6	248.1 ^a ± 0.8	37.3 ^a ± 6.6

For each sampling time, different letters indicate significant differences ($p < 0.05$) among untreated samples (C) and plasma-treated samples (P5 and P10).

Table 4 shows also the thermal parameter values related to PET material. In general, the values determined in the first scan are affected by the treatment undergone by the material during the production and use phases. These are the values that characterize the properties of the material. The values determined in the second scan give information on the intrinsic properties of the material, indicating, in this case, its tendency to recrystallize after melting and, therefore, highlighting the material behavior. In the present study, no significant differences between ΔH_m and X_c parameters were observed, indicating that the exposure to cold plasma at the applied condition did not change the materials thermal performance.

The EU regulation 10/2011 establishes that the acceptable limit for the global transfer of migrants from plastic materials intended to come into contact with food is equal to 10 mg/dm². The obtained results showed that the values of OM in PP and PET (Table 5) were well below the limits imposed by this regulation, and plasma exposure for 5 and 10 min did not modify this parameter.

Table 5. Overall migration (mg/dm²) related to the PP and PET samples.

Sample	Food Simulant	Overall Migration (mg/dm ²)	
		PP	PET
C	Acetic acid (3%)	<1	<1
C	Distilled water	<1	<1
P5	Acetic acid (3%)	<1	<1
P5	Distilled water	<1	<1
P10	Acetic acid (3%)	<1	<1
P10	Distilled water	<1	<1

The results of these tests show that controlled exposure to CAP for 5 and 10 min did not promote migration from the selected food contact materials (FCMs) beyond the permitted limits, and therefore, the applied treatments can be considered safe from this point of view.

3.5. Product Shelf-Life

Figure 6 shows the evolution of O₂ and CO₂ in the packages' headspaces during storage for all the samples, both in PET and PP. As expected, due to the respiration of the apple tissues, accumulation of CO₂ and consumption of O₂ were observed. The decrease in O₂ was faster for apples in the PET packaging, due to the higher thickness and lower permeability of this kind of material. Indeed, after only three days, the O₂ was totally consumed. However, no significant difference in CO₂ and O₂ content were found between treated (P5, P10) and control samples (C) for both packaging materials, confirming the results obtained by the permeability measurements.

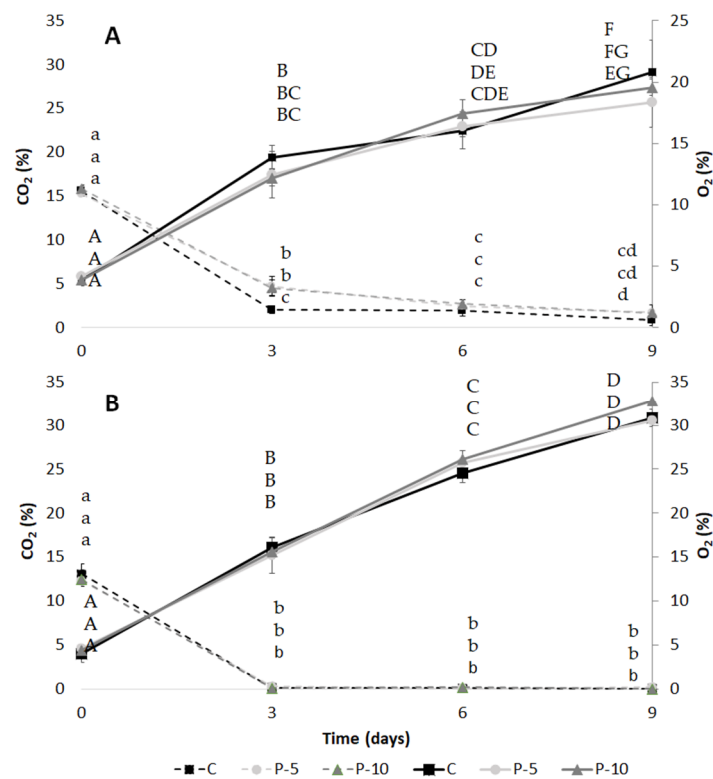


Figure 6. O₂ (dotted lines) and CO₂ (solid lines) concentration in the headspaces of PP (A) and PET (B) packages of fresh-cut apples subjected to 5 (P5) and 10 (P10) min of plasma exposure compared with the untreated ones. Different lowercase and uppercase letters indicate significant differences (*p* < 0.05) among O₂ and CO₂ values, respectively.

The color data, expressed in L (lightness) and a* (redness) of the CIE-Lab color scale, are reported in Table S1. After exposure of the packages to CAP, and during the 9 days of storage, the values remained fairly constant, with no significant differences.

Titrate acidity (TA) of apple samples and firmness values (N), measured in the apple samples during storage, are reported in Table 6.

Table 6. Titratable acidity (g/100 g) of apples packaged in PET and PP after 5 (P5) and 10 (P10) min of CAP treatment compared with the control (C) sample during 9 days of storage at 8 °C.

Sample	Storage Time (d)			
	0	3	6	9
	PET			
C	0.30 ^a ± 0.01	0.30 ^a ± 0.06	0.31 ^a ± 0.01	0.35 ^a ± 0.01
P5	0.29 ^a ± 0.00	0.29 ^a ± 0.06	0.31 ^a ± 0.06	0.33 ^a ± 0.00
P10	0.29 ^a ± 0.01	0.31 ^a ± 0.06	0.32 ^a ± 0.00	0.35 ^a ± 0.06
	PP			
C	0.20 ^a ± 0.00	0.18 ^a ± 0.06	0.20 ^a ± 0.00	0.19 ^a ± 0.06
P5	0.19 ^a ± 0.00	0.18 ^a ± 0.06	0.19 ^a ± 0.06	0.19 ^a ± 0.06
P10	0.23 ^a ± 0.05	0.22 ^a ± 0.06	0.20 ^a ± 0.06	0.19 ^a ± 0.00

For each sampling time, different letters indicate significant differences ($p < 0.05$) among untreated samples (C) and plasma-treated samples (P5 and P10).

TA showed an increase during storage in all apple samples packaged in PE; this could be related to the production of carbonic acid from CO₂, present in higher concentration in PET packages compared with PP ones. However, this difference was related to the type of material, while the exposure to CAP in both cases did not lead to any significant difference among samples.

In addition, for sample hardness data (Table S2) measured by penetration tests, results were not influenced by exposure to CAP.

Cell loads of total bacterial count, *Lactobacillus* spp., yeasts, and molds of packaged apples samples are shown in Table 7. These microbial groups were chosen because they are the main spoilage agents of minimally processed fruits and vegetables and, consequently, are able to affect the product shelf-life [23]. Although the dominance of spoilage depends on many factors, the raw material initial microbiota, the package atmosphere gas composition, and the gas permeability of packaging materials are pivotal to the determination of the relative ratios among the different microbial groups and their cell loads during storage. Otherwise, aerobic mesophilic bacteria, yeasts, lactic acid bacteria, and Enterobacteriaceae are generally used as microbial spoilage indicators of fruits to model the shelf-life of minimally processed fruits and vegetables in relation to process and storage variables [23–25].

No significant differences ($p < 0.05$) were observed among control and treated samples for both packaging materials used during storage at 8 °C. All considered microbial groups considered showed a similar trend in the samples, independent of the CAP treatment applied. Total mesophilic bacteria played the main role in the spoilage of packaged apples, followed by lactobacilli and yeasts, independent of the packaging material considered.

In fact, mesophilic bacteria attained the spoilage threshold limit of 6 log CFU/g after 6 days and 3 days in PET and PP packaging, respectively, independent of the plasma treatment applied. The limited shelf-life of the samples packaged in PP bags was mainly due to the high initial contamination values of fresh-cut apples.

Table 7. Microbial cell loads (log CFU/g) detected during 9 days of storage at 8 °C of cut apples packaged in PP and PET after 5 (P5) and 10 (P10) min of CAP treatment, compared with the control (C).

Days of Storage	Cell Loads (log CFU/g)						
	Apples in PP-Bags			Apples in PET			
	C	P5	P10	C	P5	P10	
0	TMC	4.94 ^a ± 0.29	5.15 ^a ± 0.25	5.32 ^a ± 0.28	3.40 ^a ± 0.44	3.34 ^a ± 0.62	3.83 ^a ± 0.53
	<i>Lactobacillus spp.</i>	3.23 ^a ± 0.23	3.10 ^a ± 0.34	3.12 ^a ± 0.30	2.56 ^a ± 0.22	2.81 ^a ± 0.43	2.70 ^a ± 0.22
	Yeasts	2.50 ^a ± 0.30	2.71 ^a ± 0.24	2.60 ^a ± 0.23	1.48 ^a ± 0.27	1.56 ^a ± 0.33	2.00 ^a ± 0.32
3	Molds	2.28 ^a ± 0.44	2.27 ^a ± 0.05	2.24 ^a ± 0.34	1.78 ^a ± 0.25	1.26 ^a ± 0.17	1.55 ^a ± 0.43
	TMC	6.85 ^a ± 0.34	6.92 ^a ± 0.22	6.83 ^a ± 0.25	5.45 ^a ± 0.18	4.75 ^a ± 0.37	4.56 ^a ± 0.42
	<i>Lactobacillus spp.</i>	3.05 ^a ± 0.4	3. ± 0.34	3.49 ^a ± 0.30	4.03 ^a ± 0.47	4.02 ^a ± 0.54	4.43 ^a ± 0.20
6	Yeasts	3.330 ^a ± 0.45	3.67 ^a ± 0.10	3.54 ^a ± 0.30	3.70 ^a ± 0.20	3.51 ^a ± 0.16	3.59 ^a ± 0.24
	Molds	2.18 ^a ± 0.28	2.02 ^a ± 0.34	1.93 ^a ± 0.21	*	*	*
	TMC	7.41 ^a ± 0.25	7.21 ^a ± 0.16	7.03 ^a ± 0.23	6.26 ^a ± 0.01	6.29 ^a ± 0.22	6.93 ^a ± 0.14
9	<i>Lactobacillus spp.</i>	4.18 ^a ± 0.10	3.18 ^a ± 0.18	4.21 ^a ± 0.27	4.92 ^a ± 0.59	4.80 ^a ± 0.47	4.60 ^a ± 0.28
	Yeasts	4.10 ^a ± 0.30	4.20 ^a ± 0.20	4.12 ^a ± 0.33	3.90 ^a ± 0.01	4.30 ^a ± 0.10	4.20 ^a ± 0.40
	Molds	2.30 ^a ± 0.22	2.41 ^a ± 0.20	2.58 ^a ± 0.20	*	*	*
9	TMC	8.41 ^a ± 0.25	7.75 ^a ± 0.26	7.92 ^a ± 0.23	6.91 ^a ± 0.34	6.56 ^a ± 0.17	6.89 ^a ± 0.24
	<i>Lactobacillus spp.</i>	4.55 ^a ± 0.44	4.93 ^a ± 0.46	4.27 ^a ± 0.28	6.02 ^a ± 0.08	5.45 ^a ± 0.05	5.67 ± 0.33
	Yeasts	4.60 ^a ± 0.30	4.40 ^a ± 0.30	4.60 ^a ± 0.30	4.61 ^a ± 0.10	4.23 ^a ± 0.25	4.40 ^a ± 0.20
	Molds	2.44 ^a ± 0.29	2.57 ^a ± 0.05	2.78 ^a ± 0.31	*	*	*

For each sampling time and microbial group, different letters indicate significant differences ($p < 0.05$) among untreated samples (C) and plasma-treated samples (P5 and P10); * = below the limit of determination ($< 2 \log \text{CFU/g}$).

4. Conclusions

The present study investigated the use of a newly developed plasma sanitation system for food packaging decontamination from SARS-CoV-2 RNA. Results showed that 10 min of exposure was sufficient to almost completely eliminate the extracted viral RNA from package surfaces. The treatment did not produce any significant variation in packaging material performance or the shelf-life of packaged products, indicating the potentiality of this treatment for the decontamination of packaged products.

In addition to the effect of the applied plasma treatment at the genomic level, its structural effect on the whole envelope and capsid of the actual virus needs to be assessed, while also extending this experimental approach to different packaging materials. For this reason, further studies will be undertaken in due course in our lab in order to better clarify these important aspects.

Supplementary Materials: The following are available online at <https://www.mdpi.com/article/10.3390/app11094177/s1>; Table S1. Firmness (N) value of apples packaged in PET and PP after 5 (P5) and 10 (P10) min of CAP, compared with the control (C) sample during 9 days of storage at 8 °C; Table S2. Color parameters (L^* and a^*) of apples packaged in PET and PP after 5 (P5) and 10 (P10) min of CAP, compared with the control (C) sample during 9 days of storage at 8 °C.

Author Contributions: Conceptualization, R.L. (Romolo Laurita), V.C., V.S. and P.R.; methodology, F.C., S.T., T.G. and V.S.; validation, S.T. and M.G.; formal analysis, F.C., S.T., T.G., A.C.d.A.S.P., U.T., F.S. and G.B.; investigation, F.C., S.T., T.G., A.C.d.A.S.P., U.T., F.S. and G.B.; resources, R.L. (Rosalba Lanciotti), F.G.G., V.C., V.S. and P.R.; data curation, F.C., S.T., T.G., A.C.d.A.S.P., U.T., F.S. and G.B.; writing—original draft preparation, F.C., S.T., T.G., U.T., F.S. and P.R.; writing—review and editing, R.L. (Romolo Laurita), R.L. (Rosalba Lanciotti), F.G.G., V.S., S.R., M.G., V.C., V.S. and P.R.; visualization, F.C., S.T., T.G., U.T., F.S. and P.R.; supervision, R.L. (Rosalba Lanciotti), F.G.G., S.R., V.C. and V.S.; project administration, P.R.; funding acquisition, P.R. and R.L. (Romolo Laurita). All authors have read and agreed to the published version of the manuscript.

Funding: This EIT Food activity received funding from the European Institute of Innovation and Technology (EIT), a body of the European Union, under Horizon2020, the EU Framework Programme for Research and Innovation.

Institutional Review Board Statement: Not applicable.

Informed Consent Statement: Not applicable.

Data Availability Statement: The data presented in this study are available on request from the corresponding author. The data are not publicly available due to Intellectual Property protection.

Acknowledgments: This work was supported by the COST Action TD1208: Electrical discharges with liquids for future applications. The activities were performed in the frame of the UNIBO project “Plasma technologies for biomedical, energy and environmental applications”. Permeability measurements were supported by the University of Catania, PIAAno di inCENTivi per la Ricerca di Ateneo 2020/2022, PIACERI–Linea 2, MaMex project. The authors acknowledge Alina Bisag for the 3D render of the PASS system.

Conflicts of Interest: The authors declare no conflict of interest.

References

1. Aronson, J.K. Corona Viruses—A General Introduction. Centre for Evidence-Based Medicine, Nuffield Department of Primary Care Health Sciences, University of Oxford. 2020. Available online: <https://www.cebm.net/covid-19/coronaviruses-a-general-introduction/> (accessed on 24 May 2020).
2. Anelich, L.E.; Lues, R.; Farber, J.M.; Parreira, V.R. SARS-CoV-2 and Risk to Food Safety. *Front. Nutr.* **2020**, *7*, 243. [[CrossRef](#)] [[PubMed](#)]
3. ANSES. (French Agency for Food, Environmental and Occupational Health and Safety). Opinion on an Urgent Request to Assess Certain Risks Associated with COVID-19. 2020. Available online: <https://www.anses.fr/en/system/files/SABA2020SA0037-1.pdf> (accessed on 30 April 2020).
4. Kampf, G.; Todt, D.; Pfaender, S.; Steinmann, E. Persistence of coronaviruses on inanimate surfaces and their inactivation with biocidal agents. *J. Hosp. Infect.* **2020**, *104*, 246–251. [[CrossRef](#)] [[PubMed](#)]
5. Kapoor, A.; Saha, R. Hand washing agents and surface disinfectants in times of Coronavirus (COVID-19) outbreak. *Indian J. Community Health* **2020**, *32*, 225–227. [[CrossRef](#)]
6. WHO (World Health Organization). Infection Prevention and Control During Health Care When Novel Coronavirus (nCoV) Infection is Suspected: Interim Guidance, 25 January 2020. 2020. Available online: <https://www.who.int/publications-detail/infection-prevention-and-control-during-health-care-when-novel-coronavirus-ncov-infection-is-suspected-20200125> (accessed on 20 February 2020).
7. Suman, R.; Javaid, M.; Haleem, A.; Vaishya, R.; Bahl, S.; Nandan, D. Sustainability of coronavirus on different surfaces. *J. Clin. Exp. Hepatol.* **2020**, *10*, 386–390. [[CrossRef](#)] [[PubMed](#)]
8. Alekseev, O.; Donovan, K.; Limonnik, V.; Azizkhan-Clifford, J. Nonthermal dielectric barrier discharge (DBD) plasma suppresses herpes simplex virus type 1 (HSV-1) replication in corneal epithelium. *Transl. Vis. Sci. Technol.* **2014**, *3*, 2. [[CrossRef](#)] [[PubMed](#)]
9. Liang, Y.; Wei, K.; Li, W.; Yao, M.; Zhang, J.; Grinshpun, S.A. MS2 virus inactivation by atmospheric-pressure cold plasma using different gas carriers and power levels. *Appl. Environ. Microbiol.* **2015**, *81*, 996–1002.
10. Zimmermann, J.L.; Dumler, K.; Shimizu, T.; Morfill, G.E.; Wolf, A.; Boxhammer, V.; Anton, M. Effects of cold atmospheric plasmas on adenoviruses in solution. *J. Phys. D Appl. Phys.* **2011**, *44*, 505201. [[CrossRef](#)]
11. Bisag, A.; Isabelli, P.; Laurita, R.; Bucci, C.; Capelli, F.; Dirani, G.; Gherardi, M.; Laghi, G.; Paglianti, A.; Sambri, V.; et al. Cold atmospheric plasma inactivation of aerosolized microdroplets containing bacteria and purified SARS-CoV-2 RNA to contrast airborne indoor transmission. *Plasma Process. Polym.* **2020**, *17*, 2000154. [[CrossRef](#)]
12. Chen, Z.; Garcia, G., Jr.; Arumugaswami, V.; Wirz, R.E. Cold atmospheric plasma for SARS-CoV-2 inactivation. *Phys. Fluids* **2020**, *32*, 111702. [[CrossRef](#)] [[PubMed](#)]
13. Simoncelli, E.; Schulpen, J.; Barletta, F.; Laurita, R.; Colombo, V.; Nikiforov, A.; Gherardi, M. UV–VIS optical spectroscopy investigation on the kinetics of long-lived RONS produced by a surface DBD plasma source. *Plasma Source. Sci. Technol.* **2019**, *28*, 095015. [[CrossRef](#)]
14. Moiseev, T.; Misra, N.N.; Patil, S.; Cullen, P.J.; Bourke, P.; Keener, K.M.; Mosnier, J.P. Post-discharge gas composition of a large-gap DBD in humid air by UV–Vis absorption spectroscopy. *Plasma Source. Sci. Technol.* **2014**, *23*, 065033. [[CrossRef](#)]
15. ISO 15 105-1, ASTM D1434. *Standard Test Method for Determining Gas Permeability Characteristics of Plastic Film and Sheeting*; Brugger Feinmechanik GmbH. Gas Permeability Testing Manual, Registergericht München HRB 77020; ASTM: West Conshohocken, PA, USA, 1998. [[CrossRef](#)]
16. Chakravartula, S.S.N.; Soccio, M.; Lotti, N.; Balestra, F.; Dalla Rosa, M.; Siracusa, V. Characterization of composite edible films based on pectin/alginate/whey protein concentrate. *Materials* **2019**, *12*, 2454. [[CrossRef](#)] [[PubMed](#)]
17. Siracusa, V.; Ingrao, C. Correlation amongst gas barrier behaviour, temperature and thickness in BOPP films for food packaging usage: A lab-scale testing experience. *Polym. Test* **2017**, *59*, 277–289. [[CrossRef](#)]
18. Sichina, W.J. *DSC as Problem Solving Tool: Measurement of Percent Crystallinity of Thermoplastics*. PETech-40 Thermal Analysis; Application Note; PerkinElmer Inc.: Waltham, MA, USA, 2000; Available online: <https://www.perkinelmer.com/> (accessed on 2 May 2021).

19. AOAC International. Official Methods of Analysis (OMA) of AOAC International, USA. Method Number: 942.15. 2020. Available online: <http://www.eoma.aoac.org/> (accessed on 2 May 2021).
20. Shimizu, T.; Sakiyama, Y.; Graves, D.B.; Zimmermann, J.L.; Morfill, G.E. The dynamics of ozone generation and mode transition in air surface micro-discharge plasma at atmospheric pressure. *New J. Phys.* **2012**, *14*, 103028. [[CrossRef](#)]
21. Kogelschatz, U.; Eliasson, B.; Hirth, M. Ozone generation from oxygen and air: Discharge physics and reaction mechanisms. *Ozone Sci. Eng.* **1988**, *10*, 12. [[CrossRef](#)]
22. Filipić, A.; Gutierrez-Aguirre, I.; Primc, G.; Mozetič, M.; Dobnik, D. Cold plasma, a new hope in the field of virus inactivation. *Trend. Biotechnol.* **2020**, *38*, 1278–1291. [[CrossRef](#)] [[PubMed](#)]
23. Siroli, L.; Patrignani, F.; Serrazanetti, D.I.; Tabanelli, G.; Montanari, C.; Tappi, S.; Lanciotti, R. Efficacy of natural antimicrobials to prolong the shelf-life of minimally processed apples packaged in modified atmosphere. *Food Cont.* **2014**, *46*, 403–411. [[CrossRef](#)]
24. Putnik, P.; Kovačević, D.B.; Herceg, K.; Roohinejad, S.; Greiner, R.; Bekhit, A.E.D.A.; Levaj, B. Modelling the shelf-life of minimally-processed fresh-cut apples packaged in a modified atmosphere using food quality parameters. *Food Cont.* **2017**, *81*, 55–64. [[CrossRef](#)]
25. Benner, R.A., Jr. Organisms of concern but not foodborne or confirmed foodborne: Spoilage microorganisms. In *Encyclopedia of Food Safety*; Academic Press: San Diego, CA, USA, 2014; Volume 1.